Shock and release temperatures in molybdenum: Experiment and theory

Damian C. Swift* and Achim Seifter
Group P-24, Physics Division, Los Alamos National Laboratory, MS E526, Los Alamos, New Mexico 87545, USA

David B. Holtkamp and David A. Clark
Group P-22, Physics Division, Los Alamos National Laboratory, MS D410, Los Alamos, New Mexico 87545, USA
(Received 14 April 2007; revised manuscript received 30 June 2007; published 23 August 2007)

Shock and release temperatures in Mo were calculated, taking heating from plastic flow predicted using the Steinberg-Guinan model into account. Plastic flow was calculated self-consistently with the shock jump conditions: this is necessary for a rigorous estimate of the locus of shock states accessible. Plastic heating increased monotonically with shock pressure and subsequent release, reaching an estimated 50 K at a pressure of 60 GPa, and around 120 K on release to zero pressure. The temperatures were compared with surface emission spectrometry measurements for Mo shocked to around 60 GPa and then released into vacuum or into a LiF window. Shock loading was induced by the impact of a planar projectile, accelerated by high explosive or in a gas gun. Surface velocimetry showed an elastic wave at the start of release from the shocked state; the amplitude of the elastic wave matched the prediction to around 10%, indicating that the predicted flow stress in the shocked state was reasonable. The measured temperatures were consistent with the simulations, indicating that the fraction of plastic work converted to heat was in the range 70%–100% for these loading conditions. The shock temperature predicted with plastic heating was consistent with a reanalyzed temperature from neutron resonance spectrometry.

DOI: 10.1103/PhysRevB.76.054122 PACS number(s): 62.50.+p, 62.20.Fe, 65.40.−b, 07.20.Ka

I. INTRODUCTION

The behavior of matter subjected to extreme conditions through dynamic loading is of interest from a direct physical standpoint, as dynamic loading is often the only practical way to induce extreme conditions and because important engineering problems in hypervelocity impact and weaponry involve dynamic loading.[1] Temperature is a key parameter in understanding the properties of matter, as it governs the population of vibrational processes and excitations past energy barriers. Temperature is thus important for a physical understanding of many types of behavior and the associated models. The equation of state (EOS) includes contributions from the excitation of atomic vibrations and electronic excitations. Plastic flow is mediated by the excitation of dislocations and twin boundaries past Peierls barriers. Phase changes depend on the thermodynamic state's location in the phase diagram. The kinetics of phase changes is described by the nucleation and growth of the daughter phase in the matrix of the parent phase, requiring the excitation of atoms past barriers. Chemical reactions are governed by the excitation of atoms or electrons over barriers. Diffusion in condensed matter is the motion of atoms past the barriers formed by their neighbors. Conductivities include scattering contributions from thermal excitations.

Temperature is notoriously difficult to measure during dynamic loading, in particular, for opaque materials.[2] Extreme states of matter are often hidden within a sheath of matter in a different state—this is the usual situation in shock loading experiments. Probes made of matter generally disrupt the state of interest, e.g., by presenting an impedance mismatch to compression waves. Much interesting physics in condensed matter occurs at compressions of a few tens of percent, where the heating may be in the range of a few hundred Kelvins and the resulting thermal emissions are small. Most temperature measurements of shock-loaded systems have been made using photon emission spectroscopy, commonly called pyrometry.[3,4] However, many materials of interest (e.g., metals) are opaque in the relevant region of the spectrum: infrared through visible for shocks up to the terapascal regime. Emission from an opaque material comes from the surface, which cannot be maintained at the pressure of the initial shock long enough to allow useful emission spectra to be collected. A transparent window can be placed in contact with the sample to maintain an elevated pressure, but the mismatch in shock impedance must be taken into account, along with the effect of heat conduction. Accurate temperature data have been obtained from transparent sample materials, where thermal radiation from the shocked state can escape from the sample.[5,6]

Neutron resonance spectroscopy (NRS) has been investigated as a fundamentally different technique for measuring the temperature inside a dynamically loaded specimen, which can be used on opaque materials.[7] Trial measurements of NRS temperatures were performed on shock-loaded Mo as a standard material for high pressure work; the shock temperature was found to lie significantly above the temperature predicted using reasonable EOS for Mo.[7] Measurements were also made using pyrometry of the temperature of Mo which was shocked and then released into a LiF window or into vacuum; these experiments also yielded temperatures which lie significantly above EOS predictions.[8]

Here, we consider the effect of plastic flow on the Mo pyrometry experiments. Plastic flow was neglected in previous comparisons of predictions with the temperature data. The contribution of plastic work to heating has been mentioned in studies of other metals[9] but has not been quantified in detail or consistently. The contribution to the total internal energy from plastic heating has been estimated in order to extract the scalar EOS from shock data,[10] which involves a similar analysis of shock heating, though less general.

II. CORRECTIONS AND SYSTEMATIC UNCERTAINTIES IN PYROMETRY

Polycrystalline materials, such as the Mo for which the discrepancy in temperature measurements was reported, are heterogeneous in that they are composed of an aggregate of grains of different crystallographic orientations. The Mo samples were machined from material which had been prepared by pressing from powder, so there was a population of voids and there were impurities concentrated along grain boundaries. On shock loading and subsequent release, different regions of the sample would thus respond differently, producing a variation in local temperature. Given enough time, temperature variations disperse through thermal conduction, but this typically takes an order of microseconds for grains tens of micrometers in size, which is long on the time scale of the experiments. We wish to compare pyrometry measurements of temperature in Mo with predictions using continuum models, so the temperature of interest is the mean bulk value. Thermal radiation is described by the Stefan-Boltzmann relation, where the total power is proportional to the fourth power of temperature. Pyrometry measurements are often more accurate at shorter wavelengths where the power varies with higher powers of temperature.[11] Thus, unquantified temperature variations (spatial or temporal, within the respective resolutions of the detectors) lead to an overestimate of the mean temperature. Spatial variation of brightness temperature has been observed in shock-loaded Sn,[12] which has a much lower flow stress than Mo. Thus, pyrometric measurements of temperature in heterogeneous materials are likely to be systematic overestimates of the material temperature.

Pyrometry measurements from metals probe the surface temperature. The surface is prone to increased plastic work around surface features such as machining marks: when a rough surface in contact with a material of lower impedance (or vacuum, in the extreme case) is shocked, flow may be exaggerated in pits and grooves. At sufficiently high shock pressures, localized jetting may occur. Any such localized increase in plastic flow will produce a higher local temperature, which may appear as a higher mean temperature as discussed above. Plastic work around surface features is reduced when the surface is in contact with a window. Thus, free surface release experiments are likely to exhibit larger increases of surface temperature than are window release experiments.

For experiments in which the sample is observed through a transparent window to maintain an elevated pressure, there may be additional radiation from compression of any gas or glue in the gap between the sample and the window, or from the shocked window material itself. These effects were considered and corrected for the Mo data.[13] After the shock passes from the sample into a window, the temperature of the shock state is generally different than that in the sample, so heat conduction can alter the temperature of the sample surface. In the experiments discussed here, the sample was attached to the window with Loctite Corp. type 326 glue, which has been found to produce little radiation for shock pressures of a few tens of gigapascals.[14] Care was taken to avoid leaving air gaps from sample assembly.

In multiple channel pyrometry measurements, thermal emission from the sample is recorded using a set of detectors responding to different ranges of photon wavelength. In the simplest case, a gray body spectrum can be fitted to the signals, and the mean emissivity and temperature are deduced from the shape of the spectrum. In general, the emissivity of a material varies with state and wavelength, and also with surface roughness, which may change during dynamic loading. The emissivity may be measured directly, for example, by ellipsometry. It is more common to assume that the multiple pyrometry channels oversample the wavelength variation of the radiance and emissivity, at least over a part of the spectrum, allowing both to be deduced. Again, these effects were taken into account for the Mo measurements.[13]

Aside from gaps and glues between the sample and any window, it is common for components of the shocked target assembly to include sharp corners and low-density materials such as plastics, foams, and glues as part of the engineering structure. As with glued windows, low-density materials, in general, may be shock loaded to a higher temperature than the sample. Sharp internal corners, when shocked, may form jets with large amounts of plastic heating. Thermal emission from any of these sources may be present as a background against which the emission from the sample must be distinguished. The experiments were designed to avoid conditions which could cause jetting. Some jet formation was likely out of the direct field of view of the pyrometers, but scattered radiation from jets may have contributed to the background. One possible sign of this is a background level which increases with time. Where possible, the radiance in each pyrometer channel was extrapolated to the shock breakout time to correct for time-dependent background.

The net effect of the complications associated with pyrometry measurements on metals is that it is possible to overestimate the temperature.

III. HEATING FROM PLASTIC WORK IN SHOCK AND RELEASE

After transit of a shock wave, axial and lateral release and recompression waves reverberate through the sample until it ultimately comes to rest at zero pressure. In the simplest case, which many shock physics experiments are designed to achieve, the shock is steady and planar and the initial release is planar: the material is compressed and released uniaxially. In general, the shock and release may be converging or diverging, but locally the compression and decompression induced are close to uniaxial. Specifically, the strains are not isotropic. If a crystalline solid is subjected to nonisotropic strains, then shear stresses must be induced, leading to plastic flow if the flow stress is exceeded.

In continuum dynamics situations such as shock loading, simulations and analysis may be performed accurately by a scalar solution of the shock jump and isentropic expansion relations if the material is represented by an EOS, i.e., if the effects of elasticity and plastic flow are ignored. It is a common practice to use spatially resolving numerical simulations if the material is to be represented with any greater complexity. However, simulations of shock waves are complicated by

the need to ensure that the shock—discontinuous at the continuum level—is captured accurately without inducing numerical artifacts such as oscillations or excess heating. However, numerical methods have been developed to allow shock compression and ramp decompression to be simulated by a scalar solution for general material models including elasticity and plastic flow.[15] These numerical solutions were used to interpret the temperature measurements on Mo.

Spatially resolved simulations were also performed for comparison with velocity history measurements. These simulations used a Lagrangian representation of the shock experiments, integrated in time with a predictor-corrector numerical scheme employing artificial viscosity to stabilize the shock wave.[16] The material models were identical with those used in the scalar solution.

The conservation equations for shock and release states in material dynamics are usually formulated in terms of compression and pressure. In order to take into account elastic-plastic effects, the equations were formulated in terms of the stress and strain tensors. Thus, the Rankine-Hugoniot equations[17] for conservation across the shock were expressed in terms of the total stress normal to the shock, τ_n, rather than the pressure p:

$$u_s^2 = -v_0^2 \frac{\tau_n - \tau_{n0}}{v_0 - v}, \tag{1}$$

$$\Delta u_p = \sqrt{-(\tau_n - \tau_{n0})(v_0 - v)}, \tag{2}$$

$$e = e_0 - \frac{1}{2}(\tau_n + \tau_{n0})(v_0 - v), \tag{3}$$

where v is specific volume (the reciprocal of the mass density ρ), e is specific internal energy, u_s is the speed of the shock wave with respect to the material, Δu_p is the change in material speed normal to the shock wave (i.e., parallel to its direction of propagation), and subscript 0 refers to the initial state. The specific internal energy was defined to *exclude* elastic strain energy, so the energy equation above included only the volumetric and plastic strain contributions to the volume change. The relation for adiabatic compression and release was expressed similarly as

$$\dot{e} = \begin{cases} -\dfrac{p \operatorname{div} \vec{u}}{\rho} & \text{elastic} \\ \dfrac{1}{\rho}(\|\sigma \operatorname{grad} \vec{u}\| - p \operatorname{div} \vec{u}) & \text{plastic}, \end{cases} \tag{4}$$

where τ is the stress tensor, σ the deviatoric stress,

$$\sigma \equiv \tau - \frac{1}{3}\operatorname{Tr} \tau I = \tau + pI, \tag{5}$$

$\operatorname{grad} \vec{u}$ the velocity gradient tensor, and $\operatorname{div} \vec{u}$ its trace. For uniaxial compression, $\|\sigma \operatorname{grad} \vec{u}\| = \sigma_n \partial \vec{u}_n / \partial r_n$, i.e., the product of the components in the direction normal to the wave, with all others being zero. In the non-spatially-resolved calculations, the velocity gradient was simply the assumed or imposed strain rate.

The state of the material was expressed in terms of ρ and e [allowing a mean pressure $p(\rho, e)$ to be calculated from the EOS], a deviatoric elastic strain tensor ϵ (allowing the deviatoric stress contributions σ to be calculated), and a scalar equivalent plastic strain $\tilde{\epsilon}_p$ used to calculate work hardening. As discussed elsewhere,[15] a hyperelastic formulation using strain rather than a hypoelastic formulation using stress was preferred for consistency and accuracy in situations where shear strains are applied at different compressions. Thus, the stress deviator σ was calculated from the instantaneous strain,

$$\sigma = 2G\epsilon, \tag{6}$$

where $G(\rho, T)$ is the shear modulus. Plastic flow was taken to occur using a von Mises yield surface.[18] For von Mises yield, it is necessary to calculate scalar effective magnitudes of the stress and strain tensors:

$$\tilde{\sigma} \equiv \sqrt{f_\sigma \|\sigma^2\|}, \quad \tilde{\epsilon} \equiv \sqrt{f_\epsilon \|\epsilon^2\|}, \tag{7}$$

where the factors f_ϵ and f_σ are strain and stress measures. Deformation was plastic rather than elastic if the scalar effective shear stress exceeded the yield stress $Y(\rho, e, \tilde{\epsilon}_p)$, in which case plastic strain for work hardening was accumulated at a rate

$$\dot{\tilde{\epsilon}}_p = \frac{f_\epsilon}{2} \frac{\|\dot{\epsilon}\epsilon\| + \|\epsilon\dot{\epsilon}\|}{\tilde{\epsilon}}, \tag{8}$$

where $\dot{\epsilon}$ is the deviatoric part of the symmetric part of the velocity gradient,

$$\dot{\epsilon} \equiv \dot{E} - \frac{1}{3}\operatorname{Tr} \dot{E} I, \quad \dot{E} \equiv \frac{1}{2}(U + U^T), \quad U \equiv \operatorname{grad} \vec{u}. \tag{9}$$

If $\tilde{\sigma} < Y$, the elastic deformation was simply $\dot{\epsilon}$. For uniaxial compression along the x direction, the only nonzero component of U is $[U]_{100}$.

If plastic flow occurs, then the material is always heated to some degree. Plastic flow occurs through the motion and generation of defects in the crystal lattice, such as dislocations. Usually, in polycrystalline materials, defects accumulate during plastic deformation. Heating generally represents less than the total plastic work as some potential energy is absorbed in the structure of defects. The fraction of plastic work converted to heat, f_p, has been found to depend on material, strain, and strain rate, varying between 0.3 (or less) and 1.0.[19–23] f_p is generally higher at higher strain rates and is generally taken to be 0.85–0.95 for shock loading. It was assumed here to be constant at 0.9. Thus, the contribution of plastic work to heating was

$$\dot{e}_p = f_p \frac{\|\sigma\dot{e}\|}{\rho} \tag{10}$$

if $\tilde{\sigma} > Y$, and zero otherwise.

When a metal is deformed, shear strains result in the accumulation of elastic energy until the flow stress is reached. Continued deformation results in plastic work. If the material work hardens, the rate of plastic working increases. If thermal softening occurs, the rate of plastic working decreases

but the stored elastic energy is also converted to plastic work. In an idealized material exhibiting a constant flow stress (elastic–perfectly-plastic), arbitrarily large amounts of plastic work may be accumulated by large deformations—uniaxial as well as pure shear—beyond the flow stress. Ceramics may behave differently, the flow stress decreasing to a small fraction of its initial value as deformation continues beyond the elastic limit,[9] presumably as interatomic bonds are broken and brittle damage occurs. Many transparent materials are ceramic; this reduction of the flow stress may explain why good agreement has been obtained between shock temperatures and predictions neglecting heating from the constitutive response.[6]

Plastic flow is largely irreversible. If a sample of material is shock loaded and then released,[33] the pressure reduces on release but further plastic work is done.

Mo was represented by an empirical EOS fitted to shock compression data,[24–26] with a deviatoric strength model developed and calibrated to data on the amplitude and shape of elastic waves running ahead of shocks.[24] The EOS was likely to be accurate to a few percent in temperature for the shock pressures of a few tens of gigapascals considered here. The Steinberg-Guinan strength model includes a prediction of the flow stress at elevated pressures. The flow stress, and hence the heating from plastic flow, was uncertain at the level of a few tens of percent. As discussed below, measurements of surface velocity provided an independent measure of the flow stress.

Material models for continuum dynamics are often implemented in varying ways in different computer programs. The results may depend on details such as the way in which numerical limits, e.g., on flow stress, are applied. In our simulations, the EOS was represented by an expression for pressure p in terms of mass density ρ and specific internal energy e. This is sufficient to allow the dynamical equations for the continuum to be integrated in time. Two different EOS were used, a tabular form from the SESAME library,[25] and an analytic form of the Grüneisen type. The SESAME EOS included an estimate of the electronic contribution to the heat capacity from electronic structure calculations. The Grüneisen EOS used the principal Hugoniot as its reference curve:[24] shock speed u_s in terms of particle speed u_p,

$$u_s = c_0 + s_1 u_p, \tag{11}$$

together with a relation for the Grüneisen parameter

$$\gamma(\rho) = \gamma_0 + b(\rho/\rho_0 - 1). \tag{12}$$

The shear modulus G and flow stress Y followed the Steinberg-Guinan model,[27] which includes explicit dependence on temperature T and accumulated plastic strain ϵ_p:

$$G(p,T) = G_0[1 + Ap(\rho/\rho_0)^{-1/3} - B(T - T_0)], \tag{13}$$

$$Y(p,T) = Y_0 f(\epsilon_p) G(p,T)/G_0, \tag{14}$$

$$f(\epsilon_p) = \min[(1 + \beta\tilde{\epsilon}_p)^n, Y_{\max}/Y_0]. \tag{15}$$

Because of the scaling of flow stress by shear modulus, the maximum flow stress at high pressures was not limited by the "maximum" flow stress $Y_{\max}$—this allowed the flow stress to be significantly greater than $Y_{\max}$ in the Mo impact experiments. The usual definition of the Steinberg-Guinan model[24] includes an explicit initial plastic strain from manufacture; we treated ϵ_p as a local material parameter in addition to ρ, e, and the elastic strain and set $\tilde{\epsilon}_p$ to a nonzero value in the initial conditions if required. The scalar stress and strain measures f_ϵ and f_σ were chosen for consistency with the definitions of stress and strain used in deducing strength parameters for Mo from the shock experiments used to calibrate the Steinberg-Guinan model: $f_\epsilon = f_\sigma = 3/2$.

TABLE I. Grüneisen equation of state and Steinberg-Guinan strength parameters for Mo. (From Ref. 24 with unit conversions.)

Equation of state		Strength	
ρ_0	10.2 g/cm^2	G_0	125 GPa
c_0	5.143 km/s	Y_0	1.6 GPa
s_1	1.255	A	1.14×10^{-2} GPa^{-1}
γ_0	1.59	B	1.52×10^{-4} K^{-1}
b	0.30	β	20
c_p	2.43×10^{-4} MJ/kg K	n	0.15
a	1.3	$Y_{\max}$	2.8 GPa

The SESAME EOS were defined as a pair of tables $\{p,e\}(\rho,T)$, so the $p(\rho,e)$ relation was obtained by numerical inversion and the temperature was readily calculated. Temperatures were calculated from the Grüneisen EOS with reference to a compression curve along which the temperature and specific internal energy were known, $\{T_r, e_r\}(\rho)$, and using a specific heat capacity defined as a function of density, $c_v(\rho)$ (constant in practice). The reference curve chosen was the zero Kelvin isotherm ("cold curve"), $T_r = 0$ K. This was calculated from the principal isentrope $e(\rho)|_{s_0}$ using the estimated density variation of Grüneisen parameter:

$$e_r(\rho) = e(\rho)|_{s_0} - T_0 c_p e^{a(1-\rho_0/\rho)}\left(\frac{\rho}{\rho_0}\right)^{\gamma_0 - a}. \tag{16}$$

The isentrope was calculated by numerical integration of the second law of thermodynamics,

$$\frac{\partial e}{\partial v}\Big|_s = -p(1/v, e). \tag{17}$$

Mechanical properties and temperatures calculated by either EOS gave the same result to $o(1\%)$, which constitutes good agreement for models in material dynamics. The Grüneisen EOS have slightly smoother loci, so the results presented below are from this EOS.

Simulations were performed in units of millimeters, gigapascals, microseconds, Kelvins, and Mg/m^3=g/cm^3. Parameters for Mo in these units are listed in Table I.

IV. PYROMETRY EXPERIMENTS ON MOLYBDENUM

Pyrometry measurements of the temperature in shocked and released Mo have been made using two types of experiment. In both cases, the shock was induced by the impact of a flat projectile. The projectiles were accelerated using a high

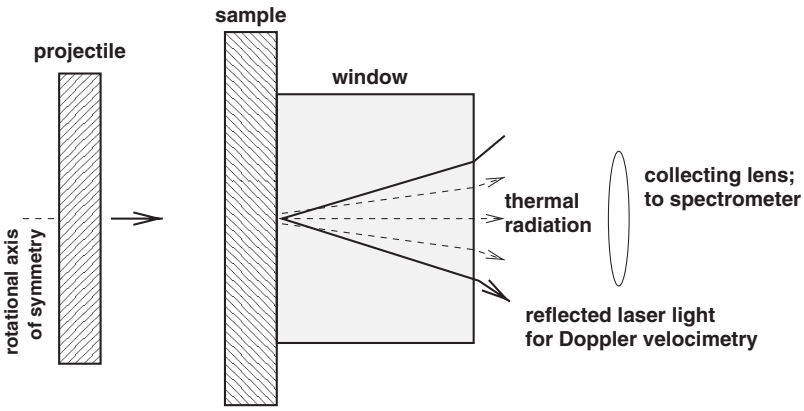

FIG. 1. Schematic of impact-induced shock experiments with surface temperature measurements. Aspect ratios are representative of the experiments discussed here. If the window is omitted, the experiment measures the free surface (zero normal stress) temperature.

explosive launcher, as in the NRS experiments, and by a gas gun. The pyrometry measurement was performed at the surface opposite the impact, the shocked state releasing either to vacuum or into a LiF window to sustain an elevated pressure (Figs. 1 and 2). In each case, the shock state was calculated using the published EOS and strength properties for the projectile and Mo target.

In all cases, the impact conditions were calculated using the scalar solution and were repeated with and without strength in all components of the impact experiment. For experiments with a LiF window, the temperature in the window was also predicted; a high temperature would signal an increased possibility of thermal radiation from the window obscuring the emissions from the Mo sample. Where an uncertainty in impact velocity was reported, the calculations were repeated for velocities at the extremes of uncertainty,

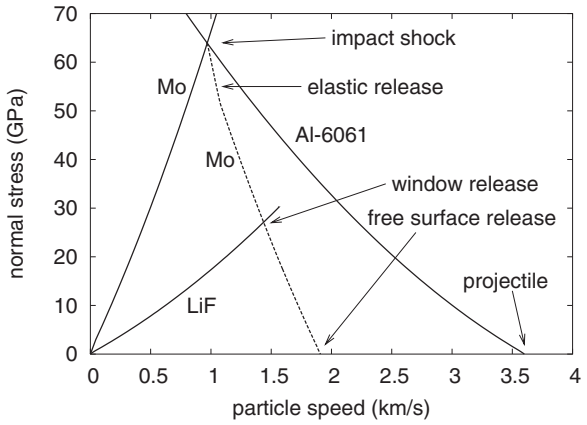

FIG. 2. Shock and release states induced in impact experiments with and without a window. Solid lines, shock Hugoniots; dashed line, release adiabat. Example calculation for Al-6061 projectile traveling at 3.6 km/s, impacting stationary Mo target and releasing into LiF window or into vacuum. The initial states of the Mo and LiF are at the origin; the initial state of the projectile is at zero normal stress and 3.6 km/s. On impact, the shock states in the projectile and sample are at the elevated pressure intersection marked "impact shock." When the shocked state in the Mo releases into the LiF window, the resulting state is the intersection marked "window release." When the shocked state in the Mo is released at a free surface, the resulting state is the zero normal stress state marked "free surface release." Release from the shocked state shows an inflection when plastic flow occurs.

giving an estimate of the uncertainty in pressure and temperature.

Similar calculations were performed with and without strength in each component separately. The Steinberg-Guinan model is least appropriate for LiF, so this is the only component where it would be useful to make such additional comparisons. However, the effect on states releasing into LiF were dominated by the strength of the Mo, so the additional comparisons are omitted for clarity. An indication that the contribution of strength in the LiF is a small effect in the simulations is that the predicted shock temperature in LiF varied much less as a function of strength than did the temperature of any of the Mo states.

Taking strength into account, on release into LiF, the normal stress in the Mo was lower than the in-plane stress because the elastic strain is a distension in the axial direction. For this reason, the calculations with strength have a lower normal stress: a result which may be counterintuitive.

The pyrometers used in these experiments used custom dichroic beam splitters to separate the collected radiation into spectral regions. For each channel, the spectral region was narrowed using a bandpass filter. Where necessary, a holographic notch filter was used to suppress stray light from the Doppler velocimetry laser, which would otherwise swamp any nearby channel. The filtered light was recorded using InSb detectors. Broadband optical components were used to allow infrared emission to be collected as well as optical emission, including CaF_2 and ZnSe lenses. Emitted radiation was collected for wavelengths up to several micrometers, providing sensitivity to surface temperatures below 500 K. These instruments are described in more detail elsewhere.[28,29]

Various improvements could be made in future pyrometry measurements to reduce the temperature uncertainties. Some optimization could be performed by repeating experiments multiple times and adjusting detector gains and digitization ranges for best accuracy. However, the difficulty and cost of each projectile impact experiment can make multiple repeats impractical.

A. Gas gun

The projectile was Ta, 3 mm thick, accelerated to 1.70 km/s using a two stage gas gun. The target was Mo, 5 mm thick. Thermal emission was measured on release into

TABLE II. Shock and release states. The Mo shock temperature measurement is from neutron resonance spectrometry, corrected for flyer curvature.

	No strength			Strength			Measured temperature (K)
	Particle speed (km/s)	Normal stress (GPa)	Temperature (K)	Particle speed (km/s)	Normal stress (GPa)	Temperature (K)	
Gas gun							
Mo shock	0.905	57.9	594	0.902	58.7	645	
Mo release into LiF	1.374	25.4	532	1.337	24.8	614	683±41
LiF shock	1.374	25.4	535	1.337	24.8	532	
Forest Flyer							
Mo shock	0.97±0.03	63.3±2.4	654±28	0.97±0.03	63.9±2.4	707±31	725±46
Mo release into vacuum	1.95±0.07	0	509±19	1.91±0.07	0	635±23	566±100
Mo release into LiF	1.48±0.04	27.8±1	581±24	1.44±0.04	27.1±1	670±25	762±40
LiF shock	1.48±0.04	27.8±1	570±17	1.44±0.04	27.1±1	566±16	624±100

a LiF window using a seven channel pyrometer.[29] The measured release temperature was 683±41 K.

The shocked state in the Mo was calculated to be 58.7 GPa and 645 K, of which 51 K was from plastic work. The state on release into LiF was thus calculated to be 24.8 GPa and 614 K, of which 82 K was from plastic work. The measured surface temperature was just 1.5 standard deviations above the temperature predicted using the Steinberg-Guinan strength model, and more than three standard deviations above the temperature predicted ignoring material strength (Table II and Fig. 3).

B. Forest flyer

The high explosive launcher used the Forest flyer design[30] used for the NRS experiments. With this system, the projectile was slightly dished on impact, though this should not affect the pyrometry measurement significantly. The projectile was accelerating slightly, reverberating elastically from the acceleration process, and possibly had a porous region through its thickness as a result of tensile stresses during acceleration. The relatively strong reverberations in the projectile affect its effective speed on impact and contributed to the uncertainty in material states.

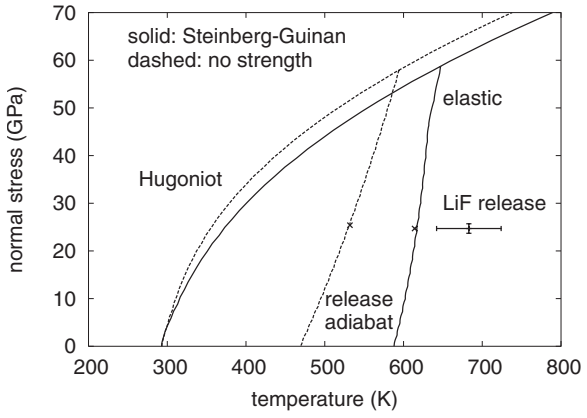

FIG. 3. Temperature measurement from a shock of 59 GPa, on release to 25 GPa into LiF, compared with predictions based on the Steinberg-Guinan strength model and with strength neglected. The crosses on the release adiabats show where release pauses when a shock is transmitted into the LiF. When strength is included, the first portion of release is elastic, the elastic portion of the adiabat is marked, and flow becomes plastic below the inflection.

The projectile was Al-6061 alloy, 6 mm thick, accelerated to 3.6±0.1 km/s. The target was Mo, also 6 mm thick. Six experiments were performed, four for release into a LiF window and two into vacuum. Surface emission was measured with a five channel visible–near-infrared pyrometer[29] or a four channel near infrared pyrometer.[28] The free surface temperature had a relatively large uncertainty, and the signals on release into LiF showed evidence of thermal emission from the LiF itself with a temperature of around 580 K.[13] The measured release temperatures were 762±40 K into LiF and 568±100 K from the free surface.

The shocked state in the Mo was calculated to be 63.9±2.4 GPa and 707±31 K, of which 53±3 K was from plastic work. The state on release into LiF was thus calculated to be 27.1±1 GPa and 670±25 K, of which 89±1 K was from plastic work. The state on release into vacuum was calculated to be 635±23 K, of which 126±4 K was from plastic work. The uncertainties are correlated: the smallest, mean, and largest of each go together.

The surface temperature on release into LiF was 1.5–2.5 standard deviations of the temperature predicted using the Steinberg-Guinan strength model and 3.5–4.5 standard deviations from the temperature predicted without strength. The uncertainty in the free surface release temperature was too large to discriminate between a purely hydrodynamic calculation (no strength) and the Steinberg-Guinan model—both lie within one standard deviation of the measurement. The predicted temperature of the LiF itself also matched the measurement to within the experimental uncertainties (Table II and Fig. 4).

The velocity history of the surface of the sample was measured by laser Doppler velocimetry of the VISAR type.[31] General features of the velocity history included a rapid acceleration when the shock reached the surface, a roughly constant peak velocity corresponding to the sustained pres-

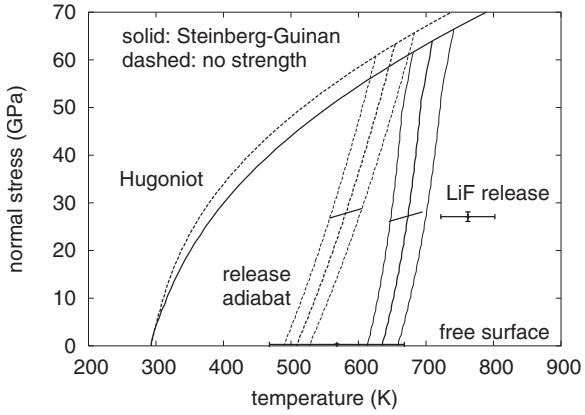

FIG. 4. Temperature measurements from a shock of 64 GPa, on release to 27 GPa into LiF and to zero pressure, compared with predictions based on the Steinberg-Guinan strength model and with strength neglected. The release adiabat from the mean shock pressure is shown, along with adiabats reflecting the uncertainty in shock pressure. The lines across the release adiabats show where release pauses when a shock is transmitted into the LiF.

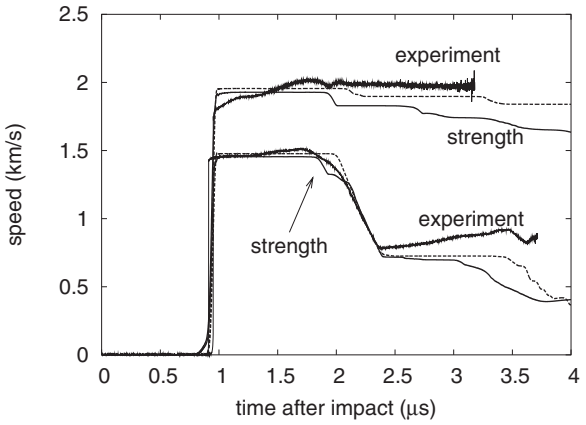

FIG. 6. Surface velocity history in Forest flyer impact experiment with a free surface (upper traces) and a LiF window (lower traces). Each experimental record is compared with two continuum dynamics simulations, with (solid lines) and without (dashed lines) strength in the Mo. The elastic precursor to the release wave is evident where the experimental velocity histories deviate from the simulations without strength.

sure behind the shock, deceleration caused by the release wave from the rear of the projectile, and a slight reacceleration as the sample was subjected to tensile stress causing spall-type damage (Fig. 5). The epoch of peak velocity was not perfectly constant but showed some acceleration. This was probably caused by the compression gradient in the projectile from the residual accelerating pressure at impact, and any regions of porosity resulting from tensile damage as the projectile was accelerated by the relatively strong pressures induced by the detonating high explosive. The onset of release showed a clear elastic precursor (Fig. 6).

The measured velocity histories were compared with spatially resolved one-dimensional continuum dynamics simulations. The projectile was modeled as ideal, i.e., at uniform STP conditions and traveling at a constant speed of 3.6 km/s with no reverberations. As a result, the peak velocity epoch was flatter than measured, but was in good agreement for amplitude and duration. Release into the LiF was also reproduced well overall. The shape of the elastic precursor to release was not reproduced perfectly using the Steinberg-Guinan strength model, but its amplitude was reproduced to within around 10% and the time of arrival was in good agreement with the experiment. The difference in shape could be caused by inadequacy in the Steinberg-Guinan model—for example, in the detailed work-hardening history in the shocked state—but is more likely to reflect density variations in the projectile as discussed above. The uniaxial strains greatly exceeded the elastic limit on release as well as on compression, so the plastic work should be dominated by the flow stress rather than the precise path before plastic flow occurred. Thus, the agreement between calculated and observed amplitudes suggests that the plastic work should be correct to around 10%.

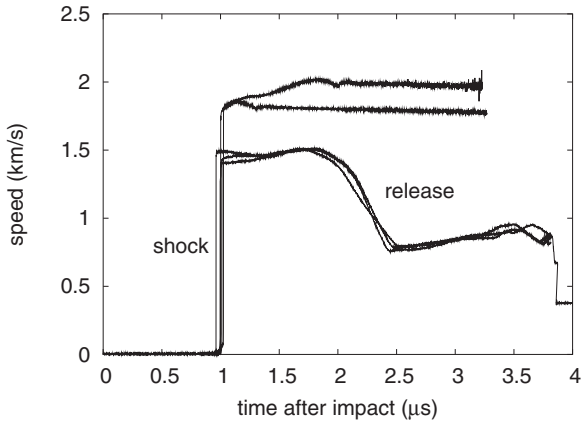

FIG. 5. Surface velocity histories measured in Forest flyer impact experiments with and without a LiF window. Separate lines are from different experiments. The upper two traces are from free surface release; the lower three are from release into a LiF window.

The calculated temperature in the shocked Mo was in good agreement with the NRS temperature measurements, once the NRS data were corrected for curvature of the flyer[32] (Fig. 7).

Spallation did not affect the shock and release states of interest for the temperature measurements considered here. The simulations used a crude spall model of the minimum pressure type, with a minimum pressure of −1.5 GPa,[24] meaning that the maximum tensile stress induced by the Mo as it was distended was 1.5 GPa. No treatment of accumulating porosity was included, so the Mo as simulated continued to exert a tensile stress when, in reality, voids or cracks would open, reducing the stress. Thus, the simulations of velocity history did not show a reacceleration after the deceleration associated with the release wave. Tensile damage and spall can depend strongly on the strain rate and loading history. The simulated and observed release decelerations matched to within a few percent, suggesting that the published spall strength applies well to the loading history induced by these projectile impact experiments.

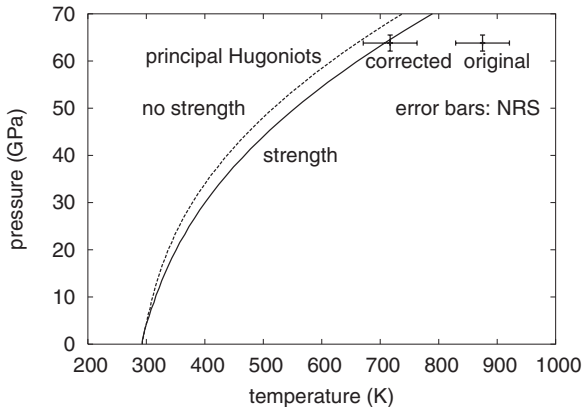

FIG. 7. Comparison between shock Hugoniot with and without strength and neutron resonance spectrometry measurements of initial shock temperature in Mo in the explosively launched flyer experiments.

V. CONCLUSIONS

Shock and release temperatures were calculated self-consistently using the equation of state and a published constitutive model for Mo. Strength was calculated to make a significant difference to states in experiments exploring pressures of tens of gigapascals. The high pressure flow stress predicted using the Steinberg-Guinan strength model matched the elastic release precursor observed using surface Doppler velocimetry, suggesting that the flow stress was correct to around 10%. The predicted temperatures were consistent with pyrometry measurements for shocks of around 60 GPa, releasing into a LiF window or into vacuum. The LiF release temperatures were clearly more consistent with plastic work as predicted using the Steinberg-Guinan model than with hydrodynamic flow (no strength). The uncertainties in temperature were, however, too large to discriminate between strength models to better than several tens of percent in flow stress.

Heating from plastic work was calculated to be around 50 K for shock pressures around 60 GPa, 90 K on subsequent release into LiF, and 125 K on release at a free surface. The fraction of plastic work converted to heat was assumed to be 90%—the heating would have been about 10% greater if all the plastic work appeared as heat. Taking plastic flow into account, the discrepancy between predictions and measured release temperatures for Mo was largely eliminated. This is a validation of the models of EOS and strength for Mo and of the use of pyrometry to measure release temperatures in metals—though the pyrometry measurements obtained in these experiments were not precise enough to discriminate between models calibrated against similar mechanical data such as velocity histories. The fraction of plastic work converted to heat was most likely to be close to 100%, though the uncertainty in the temperature measurements means that this figure cannot be justified statistically to better than a few tens of percent.

Plastic flow makes a significant contribution to reconciling the temperature discrepancy observed in the NRS experiments on shocked Mo. The calculated shock temperature including plastic heating matches the NRS data once corrected for curvature of the flyer, to which the initial NRS experiments were particularly sensitive.

ACKNOWLEDGMENTS

We would like to acknowledge the contribution of Carl Greeff for assistance and advice on equations of state and their uncertainties or certainties for Mo, of Ron Rabie, David Funk, Rob Hixson, and Chuck Forest for detailed information on the design and testing of the Forest flyer loading system, and of Sheng-Nian Luo for general advice and comments on pyrometry and material dynamics. The gas gun experiments were performed by D. B. Holtkamp, P. Paulsen, P. Fiske, D. DeVore, J. Garcia, and L. Tabaka at Lawrence Livermore National Laboratory in 1999. The work was performed under the auspices of the U.S. Department of Energy under Contracts No. W-7405-ENG-36 and No. DE-AC52-06NA25396.

*dswift@lanl.gov

[1] M. Eremets, *High Pressure Experimental Methods* (Oxford University Press, New York, 1996).
[2] S.-N. Luo and D. C. Swift, Physica B **388**, 139 (2007).
[3] S. B. Kormer, Sov. Phys. Usp. **21**, 689700 (1965).
[4] M. B. Boslough and T. J. Ahrens, Rev. Sci. Instrum. **60**, 3711 (1989).
[5] S.-N. Luo, J. A. Akins, T. J. Ahrens, and P. D. Asimow, J. Geophys. Res. **109**, B05205 (2004).
[6] S.-N. Luo, D. C. Swift, R. N. Mulford, N. D. Drummond, and G. J. Ackland, J. Phys.: Condens. Matter **16**, 5435 (2004).
[7] V. W. Yuan, J. D. Bowman, D. J. Funk, G. L. Morgan, R. L. Rabie, C. E. Ragan, J. P. Quintana, and H. L. Stacy, Phys. Rev. Lett. **94**, 125504 (2005).
[8] A. Seifter, K. Boboridis, D. A. Clark, R. B. Corrow, D. B. Holtkamp, G. L. Morgan, J. R. Payton, P. Quintana, C. E. Ragan, P. Rodriguez, H. L. Stacey, W. S. Vogan, V. W. Yuan, and A. W. Obst, in Proceedings of the 9th International Symposium on Temperature Measurements in Industry and Science (TEMPMEKO), Vol. 2, edited by D. Zvizdic, L. G. Bermanec, T. Veliki, and T. Stasic (Laboratory for Process Measurement, Faculty of Mechanical Engineering and Naval Architecture, Zagreb, Croatia, 2004), p. 1185.
[9] S. A. Raikes and T. J. Ahrens, Geophys. J. R. Astron. Soc. **58**, 717 (1979).
[10] C. E. Morris and J. N. Fritz, J. Appl. Phys. **51**, 1244 (1980).
[11] A. Seifter and A. Obst, Int. J. Thermophys. **28**, 54 (2007).
[12] A. Seifter (unpublished).
[13] A. Seifter and D. C. Swift (unpublished).
[14] D. Partouche-Sebban, J. L. Pélissier, F. G. Abeyta, W. W. Anderson, M. E. Byers, D. Dennis-Koller, J. S. Esparza, R. S. Hixson, D. B. Holtkamp, B. J. Jensen, J. C. King, P. A. Rigg, P. Rod-

riguez, D. L. Shampine, J. B. Stone, D. T. Westley, S. D. Borror, and C. A. Kruschwitz, J. Appl. Phys. **97**, 043521 (2005).
[15] D. C. Swift, arXiv:0704.0008.
[16] D. Benson, Comput. Methods Appl. Mech. Eng. **99**, 235 (1992).
[17] For a recent review and introduction, see, e.g., M. R. Boslough and J. R. Asay, in *High-Pressure Shock Compression of Solids*, J. R. Asay and M. Shahinpoor (Springer-Verlag, New York, 1992).
[18] R. Hill, *The Mathematical Theory of Plasticity* (Clarendon, Oxford, 1950).
[19] W. S. Farren and G. I. Taylor, Proc. R. Soc. London, Ser. A **107**, 422 (1925).
[20] H. Quinney and G. I. Taylor, Proc. R. Soc. London, Ser. A **163**, 157 (1937).
[21] J. J. Mason, A. J. Rosakis, and G. Ravichandran, Mech. Mater. **17**, 135 (1994).
[22] R. Kapoor and S. Nemat-Nasser, Mech. Mater. **27**, 1 (1998).
[23] J. Hodowany, G. Ravichandran, A. J. Rosakis, and P. Rosakis, Exp. Mech. **40**, 113 (2000).
[24] D. J. Steinberg, Lawrence Livermore National Laboratory Report No. UCRL-MA-106439, 1996 (unpublished).
[25] K. S. Holian, Los Alamos National Laboratory Report No. LA-10160-MS, 1984 (unpublished).
[26] C. Greeff (unpublished); (private communications).
[27] D. J. Steinberg, S. G. Cochran, and M. W. Guinan, J. Appl. Phys. **51**, 1498 (1980).
[28] K. Boboridis and A. W. Obst, *in Temperature: Its Measurement and Control in Science and Industry*, edited by D. C. Ripple (American Institute of Physics, New York, 2003), Vol. 7, Pt. 2, p. 759.
[29] D. B. Holtkamp (unpublished).
[30] D. C. Swift, C. A. Forest, D. A. Clark, W. T. Buttler, M. Marr-Lyon, and P. Rightley, Rev. Sci. Instrum. **78**, 063904 (2007).
[31] L. M. Barker and R. E. Hollenbach, J. Appl. Phys. **43**, 4669 (1972).
[32] D. C. Swift, A. Seifter, D. B. Holtkamp, V. W. Yuan, D. Bowman, and D. A. Clark, arXiv:0707.0040.
[33] In purely hydrodynamic analyses, where the effect of plastic flow is ignored, release from a shocked state follows an isentrope. This is no longer true when additional dissipative processes occur, such as plastic flow and viscosity, which lead to heating with an increase in entropy. The term "quasi-isentropic" is sometimes used in this context, particularly for shockless compression; here, we prefer to refer to the release loci as adiabats since this is a more specific term.